Journal of Reports in Pharmaceutical Sciences 2015, 4(1), 82-100

A Linear Principal Component Regression and Nonlinear Neural Network Model for Determination of Indomethacin in Plasma Samples Using UV-Vis Spectroscopy and Comparison with HPLC

Gholamreza Bahrami[a], Hamid Nabiyar[b], Komail Sadr Javadi[c], Mohsen Shahlaei[d*]

[a]Medical Biology Research Center, Kermanshah University of Medical Sciences, Kermanshah, Iran.
[b]Student Research Committee, Kermanshah University of Medical Sciences, Kermanshah, Iran.
[c]Pharmaceutical Sciences Research Center, Faculty of Pharmacy, Kermanshah University of Medical Sciences, Kermanshah, Iran.
[d]Nano Drug Delivery Research Center, Kermanshah University of Medical Sciences, Kermanshah, Iran.

ARTICLE INFO

Article Type:
Research Article

Article History:
Received: 2015-04-09
Revised: 2015-06-05
Accepted: 2015-06-20
ePublished: 2015-06-28

***Keywords*:**
Principal Component analysis
Artificial Neural Network
Indomethacin
HPLC

A B S T R A C T

A sensitive and selective method using combination of two chemometrics methods, principal component Analysis (PCA) and artificial neural network (ANN), and UV-Visible spectroscopy has been developed for the determination of Indomethacin (IDM) in plasma samples**.** Initially the absorbance spectra were processed using PCA to noise reduction and data compression. The scores of these PCs were used as the inputs of ANN. The ANN trained by the back-propagation learning was employed to model the complex non-linear relationship between the PCs extracted from UV-Visible spectra of IDM and the absorbance values. Nonlinear method (PC-ANN) was better than the PCR method considerably in the goodness of fit and predictivity parameters and other criteria for evaluation of the proposed model.
Optimal ANN model were as follows: Number of input PCs: 2, number of neurons in hidden layer: 3. The linear calibration range was 1×10^{-7} to 2.4×10^{-6} M, the detection limit were 0.21×10^{-7} M., The results have been compared with those obtained by the HPLC method.

*Corresponding Author: Mohsen Shahlaei,E-mail: mohsenshahlaei@yahoo.com

Introduction

Non-steroidal anti-inflammatory drugs (NSAIDs) suppress pain and inflammation in rheumatoid and psoriatic arthritis by inhibiting cyclooxygenases-mediated prostaglandin synthesis. Recently, some NSAIDs have been implicated in cancer chemotherapy and chemoprevention. Indomethacin is a NSAID and antiphlogistic in common use.

A number of analytical methods for the quantitative determination of indomethacin in biological fluids and samples have been reported in literature. These methods have included liquid chromatography with UV (LC–UV) [1-8] and fluorometric detection [9] as well as liquid chromatography–mass spectrometry (LC–MS/MS) [10].

Multivariate calibration methods (such as partial least squares (PLS) or principal component regression (PCR)) can be used to determination of drugs in biological fluids [11-13].

These methods can allow spectrophotometric determination of drugs in biological fluids as well as improve the data handling process of complex chemical systems [14].

In one hand, PCR is capable of being a full-spectrum technique and consequently enjoys the signal averaging of other full-spectrum techniques such as PLS and classical least squares (CLS). On the other hand, PCR also has characteristics and advantages of the inverse least squares (ILS) method, which is limited in the number of spectral wavelengths that can be applied in the analysis [15]. The application of PCR has a few advantages. At first, there is one common set of principal components for all analytes. This simplifies the supervised and unsupervised learning and interpretation and enables a simultaneous graphical inspection. Secondly, when the analyte concentrations are strongly correlated one may expect that the PCR model is more robust than conventional multivariate regression model.

The linear multivariate calibration methods such as PCR are not suitable when non-linearity is observed in the system of interest. Artificial neural networks (ANNs) technique has several benefits over the conventional multivariate calibration of data including effortlessly programming of the network architecture, not requirement for any priori assumption on the behavior of the data, capability to process input data containing some degree of uncertainty and handling non-linearity due to analyte–analyte interaction, the synergistic effect and so on [16].

Due to these benefits ANNs have attracted the interest of many researches in the field of analytical chemistry as modeling tools for multivariate calibrations [11-13, 15, 16].

Among neural networks, the most popular is the multi-layer feed-forward neural networks with the back-propagation learning algorithm.

Materials and Methods

Chemicals, Instruments and software

Pure powder of IDM was purchased from sigma. HPLC grade acetonitrile and chloroform was obtained from Merck. Stock solutions (10^{-3} M) of IDM for recording UV-Vis absorbance spectra were prepared in chloroform. All other chemicals used were of analytical grade quality and bidistilled water was used too. An hp spectrophotometer (Agilent 8453) with 10 mm quartz cells was used. A PCA and ANN required routines were written in Matlab package in our laboratory. The concentration of the mixture solutions were uniformly distributed over the range from 1×10^{-7} to 2.4×10^{-6} M. The UV–visible spectra of the mixtures were used over the wavelength range 300–400 nm in increments of 1nm.

Sample extraction

The plasma samples were stored at −20 ˚C and allowed to thaw at room temperature before processing. The analyte of interest (IDM) was extracted from the plasma samples using a single-step liquid-liquid extraction procedure. 1 ml clean human plasma samples were pipetted into clean glass tubes and analytes with known concentration was added. The tube then was vortex-mixed for 2 min and allowed to stand at room temperature for some minute. Subsequently,

the samples was treated with 1 µl HCL 2M and shake well. A total of 2 ml chloroform was added. After vortexing for 3 min, and after 20 min centrifugation at 6000 rpm, the organic phase was transferred into a new glass tube and evaporated until completely dry under a nitrogen stream.

Univariate calibration

In order to find the linear dynamic concentration range of IDM, a univariate calibration was carried out. Different volumes of a 1×10^{-4} solution of IDM added into different 10 ml volumetric flasks and diluted to the mark with plasma. An extraction procedure described above was used. The absorbance spectra were recorded over the 190–1100 nm spectral range versus a solvent blank. However, the absorbance spectra were used over the 300–400 nm. The linear dynamic range for IDM was determined by plotting the absorbance at its λ_{max} (323 nm) versus sample concentration.

Standard Solutions in Plasma

To build chemometrics models, a set of standard solutions (i.e. training and test sets), plasma spiked with IDM within the linear dynamic ranges were prepared.

As shown in Table 1, the calibration set contained 40 standard solutions, and 26 mixtures were employed in the validation set. The respective concentrations of IDM in the standard mixtures were in their linear range. For preparation of each solution, the required volumes of stock solution were added to a 10.0 ml volumetric flask, and the contents of the flask were diluted to volume with solvent. Then, the absorbance spectra of the mixture were recorded versus the solvent blank. The spectra were recorded in the wavelength range of 190–1100 nm but the range of 280–400 nm was used in the calibration step.

Calibration and validation sets splitting

In order to test the final model performances, about 45% of the samples (26 out of 66) were selected as external test set samples. The best situation of this step of model formation is dividing original matrix of absorbance spectra to guarantee that both training and test sets individually cover the total splitting of dataset as each of samples in test set is close to at least one of the samples in the training set. Various methods were used as tools for splitting the whole original dataset to the training and test sets. According to Tropsha, the best models would be built when Kennard and Stone algorithm was used [17].The Kennard–Stone [18] algorithm selects a set of samples in studied set of data, which are 'uniformly' distributed over the space defined by the original dataset.

This is a classic technique to extract a representative set of samples from a given dataset. In this technique the samples are selected consecutively. The first two samples are chosen by selecting the two farthest apart from each other. The third sample chosen is the one farthest from the first two samples, etc. Supposing that m samples have already been selected (m<n), the (m+1)th sample in the calibration set is chosen using the following criterion:

$$\max_{m<r\leq n}(\min(d_{1r}, d_{2r}, \ldots d_{mr})$$

where n stands for the number of samples in the training set, d_{jr} ; j=1,...,m are the squared euclidean distances from a candidate sample *r*, not yet included in the representative set, to the m samples already included in the representative set. One more benefit of the Kennard–Stone method is that it may be used to any matrix of predictors; there are no restrictions regarding the matrix multicollinearity. The other advantage is that the test samples all fall inside the measured region and the training set samples map the measured region of the input variable space completely with respect to the induced metric.

Table 1. Concentration data of the original dataset for studied samples of IDM spiked in plasma.

Sample No.	Concentration	Sample No.	Concentration	Sample No.	Concentration
1	1.00×10^{-7}	23	6.00×10^{-7}	45	1.30×10^{-6}
2	1.25×10^{-7}	24	6.25×10^{-7}	46	1.35×10^{-6}
3	1.50×10^{-7}	25	6.50×10^{-7}	47	1.40×10^{-6}
4	1.75×10^{-7}	26	6.75×10^{-7}	48	1.45×10^{-6}
5	2.00×10^{-7}	27	7.00×10^{-7}	49	1.50×10^{-6}
6	2.25×10^{-7}	28	7.25×10^{-7}	50	1.55×10^{-6}
7	2.50×10^{-7}	29	7.50×10^{-7}	51	1.60×10^{-6}
8	2.75×10^{-7}	30	7.75×10^{-7}	52	1.65×10^{-6}
9	3.00×10^{-7}	31	8.00×10^{-7}	53	1.70×10^{-6}
10	3.25×10^{-7}	32	8.25×10^{-7}	54	1.75×10^{-6}
11	3.50×10^{-7}	33	8.50×10^{-7}	55	1.80×10^{-6}
12	3.75×10^{-7}	34	8.75×10^{-7}	56	1.85×10^{-6}
13	4.00×10^{-7}	35	9.00×10^{-7}	57	1.90×10^{-6}
14	4.25×10^{-7}	36	9.25×10^{-7}	58	1.95×10^{-6}
15	4.50×10^{-7}	37	9.50×10^{-7}	59	$2.00\times^{10-6}$
16	4.75×10^{-7}	38	9.75×10^{-7}	60	2.05×10^{-6}
17	5.00×10^{-7}	39	1.00×10^{-6}	61	2.10×10^{-6}
18	5.25×10^{-7}	40	1.05×10^{-6}	62	2.15×10^{-6}
19	5.50×10^{-7}	41	1.10×10^{-6}	63	2.20×10^{-6}
20	5.25×10^{-7}	42	1.15×10^{-6}	64	2.25×10^{-6}
21	5.50×10^{-7}	43	1.20×10^{-6}	65	2.30×10^{-6}
22	5.75×10^{-7}	44	1.25×10^{-6}	66	2.40×10^{-6}

Principal Component Analysis (PCA)

Multivariate calibration methods are important applications in multicomponent spectrophotometry. Let ***A*** and ***C*** represent the matrices of absorbance and the concentration of a set of standard solutions containing plasma spiked with IDM, respectively. Then their absorbances are measured at *l* wavelengths, the following equation applies:

$$\boldsymbol{A}_{\mathrm{m}\times\mathrm{l}} = \boldsymbol{C}_{\mathrm{m}\times\mathrm{n}}\boldsymbol{K}_{\mathrm{n}\times\mathrm{l}}$$

where ***K*** is the coefficient matrix. According to this equation, it is possible to determine the principal components individually with the application of suitable chemometric techniques [19].

PCR is principal component multivariate mathematical tools, which have been successfully applied to analysis of multicomponent mixtures. As with the more conventional classical least squares method, PCR also need a calibration step where chemometrics model is generated on the basis of the measured spectra and relevant component concentrations of the standard samples. Spectra of the unknown solutions are then compared with the calibration set to predict the concentrations of the validation and subsequently the unknown samples.

Experimental spectrums were exported to the MATLAB routines for the purpose of PCA. The complete data set, defined by the absorbance of drugs in the columns (in this study, 101 columns) and the samples in the rows, was autoscaled through mean centering by column. PCA models the maximum directions of variation in a data set by projecting the samples as a swarm of points in a space spanned by PC's. Each PC is a linear

function of a number of original absorbance of drugs, resulting in a reduction of the original number of variables. PC's describe, in decreasing order, the most variation among the samples, and because they are calculated to be orthogonal to one another, each PC can be interpreted independently. This allows an overview of the data structure by revealing relationships between the samples as well as the detection of deviating samples. To find these sources of variation, the original data matrix of UV-Visible spectrums, defined by X(n,m), is decomposed into the sample space, the descriptor space, and the error matrix. The latter represents the variation not explained by the extracted PC's and is dependent on the problem definition. The approach describing this decomposition is presented as:

$$A(m,l) = T(m,k)P(k,l)^T + E(m,l)$$

Where *X* is the independent absorbance matrix, T is the scores matrix, P is the loadings matrix, E is the error matrix, *n* is the number of samples, *m* is the number of rows in original data set, and *k* is the number of PC's used.
In PCR procedure, all calculated scores were collected in a single data matrix and the best subset of PCs was obtained by a stepwise regression.

Artificial neural network

One method to providing a more flexible form of linear regression is to use a feed-forward neural network with error back-propagation learning algorithm. This is a computational system whose design is based on the architecture of biological neural networks and which consists of artificial 'neurons' joined so that signals from one neuron can be passed to many others (Figure 1). Clarification of the theory of the artificial neural networks in details has been adequately described elsewhere [20]but little relevant remarks is presented. ANN are parallel computational tools consisting of computing units named neurons and connections between neurons named synapses that are arranged in a series of layers.

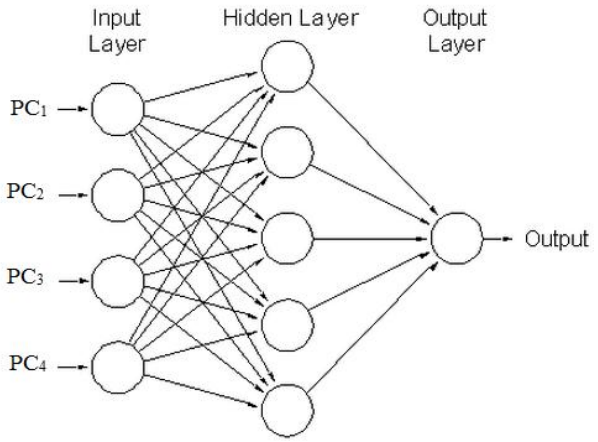

Fig.1. Typical architecture of artificial neural network

Back propagation artificial neural network includes three layers. The first layer namely input layer has n_i neurons, and duty of this layer is reception of information (i.e. inputs) and transfers them to all neurons in the next layer called the hidden layer that number of them was indicated by n_h. The neurons in the hidden layer calculate a weighted sum of the inputs that is subsequently transformed by a linear or non-linear function. The last layer is the output layer and its neurons handle the output from the network and it is the calculated response vector. Duty of synapses is connection of input layer to hidden layer and hidden layer to output layer. The manner in which each node transforms its input depends on the "weights" and bias of the node, which are modifiable. On the other hand the output value of each node depends on both the weight, and biases values. In addition, depend on, the weighted sum of all network inputs, which are normally transformed by a nonlinear or linear transform function determine the outputs of the network.

The relation between response, Y_O, of the network and a vector input, X_i, can be written as following if number of neurons in the output layer is equal to 1 (same with our condition in here):

$$Y_O = \sum_{J=1}^{N_H} W_J \, f\left(\sum_{I=1}^{N_I} W_{JI} X_I + b_I \right) (1)$$

Where $b_j$is the bias term, W_{JI} is the weight of the connection between the Ith neuron of the input layer and the Jth neuron of the hidden layer, and f

is the transformation function of the hidden layer. In the training process, the weights and bias of the network which are the adjustable parameters of the network are determined from a set of objects, which is known as training set.

Through the training of the network, the connection weights are regulated so that error of calculated responses and observed values was minimized. For this, a nonlinear transfer function makes a connection between the inputs and the outputs. Commonly neural network is adjusted, or trained, so that a particular input leads to a specific target output. There are numerous algorithms available for training ANN models. We used back propagation algorithm here for training of network. In this algorithm several steps for minimizing of networks were performed and the update of weight for the *(n + 1)*th pattern is given as:

$$W_{JI,n+1} = W_{JI,n} + \alpha \Delta W_{JI,n} \quad (2)$$

With using following equation the descent down the error surface is calculated:

$$\Delta W_{JI,n} = -\mu \frac{\partial E}{\partial W_{JI,n}} \quad (3)$$

Where α and μ are momentum and learning rate, respectively.

With respect to above demonstration, in the ANN some adjustable parameters exist including number of nodes in input and hidden layers, transfer function of hidden and transfer function output layers, momentum, number of iteration for training of network and learning rate that were evaluated by obtaining those which result in minimum in the error of prediction.

As mentioned above in order to avoid overfitting and underfitting, a validation set was used in the ANN modeling. Evaluation of ANN was performed on an external set (validation set) that consisted of samples belonging to neither the calibration set nor the test set.

High-performance liquid chromatography

The HPLC system consisted of two pumps (LC-10AD), a column oven (CTO-10A), a UV–vis spectrophotometer detector (SPD-10AD) operated at wavelength of 220 nm, a degasser (DGU-3A) and a data processor (C-R4A) all from Shimadzu, Kyoto, Japan. Chromatographic separation was achieved using a Shim-pack CLC-ODS analytical column (125 mm × 4 mm I.D.) which was packed with 5 µm particles and a Shim-pack G-ODS guard column (1 cm × 4.0 mm I.D., 5 µm particle size). The column oven temperature was set at 50 °C and the mobile phase was filtered, degassed and pumped at a flow rate of 1.8 ml/min with backpressure of 95kg/cm^2.

The injection volume was 20 µL for all the solutions and the detection was performed at the wavelength of 220 nm.

The composition of the mobile phase was varied to resolve the chromatogram of IDM. The mobile phase solvent comprising acetonitrile/water with the volume ratio of 47/53 produced better separation of the chromatograms.

In order to determine the concentration of IDM in human serum using HPLC, an extraction method was used applying hexane. Plasma samples were spiked with appropriate amounts of standard solutions, resulting in an IDM concentration range from 1.40×10^{-8} to 6.98×10^{-8}M. Aliquots of blank, calibration standard or test human plasma samples (50 µL) were pipetted into separate Eppendorf tubes, containing different concentration of IDM. Subsequently, the samples was treated with 50 µl HCL 0.1M and shake well. The samples were extracted with 1.5 mL of hexane, after vortex mixing for 60 s. the organic phase was separated and its evaporation at 45°C under the nitrogen flow. Then, samples were solved in 100 µl acetonitrile and shake well again and injected in HPLC.

The calibration equation was H = 1257c + 0.8807 (R^2 = 0.976), where *H* is the analyte height and c its concentration in M. Calibration curves were obtained by linear least-squares regression analysis plotting of peak-height versus the IDM concentrations. For the analysis of real samples containing IDM, appropriate dilutions were made with mobile phase, before filtering and injecting them into the chromatograph.

Results and discussion

Conventional univariate calibration

Fig. 2 shows the absorption spectra of IDM extracted from plasma. Fig. 2 shows that the absorbance maximum of IDM is at 323 nm.

To ensure of linear behavior and to obtain the linear dynamic range of IDM, a set of samples in different concentrations was prepared and under the optimum conditions absorbance spectra was recorded. The individual calibration curve was constructed with several points at peak of absorbance (figure 2).

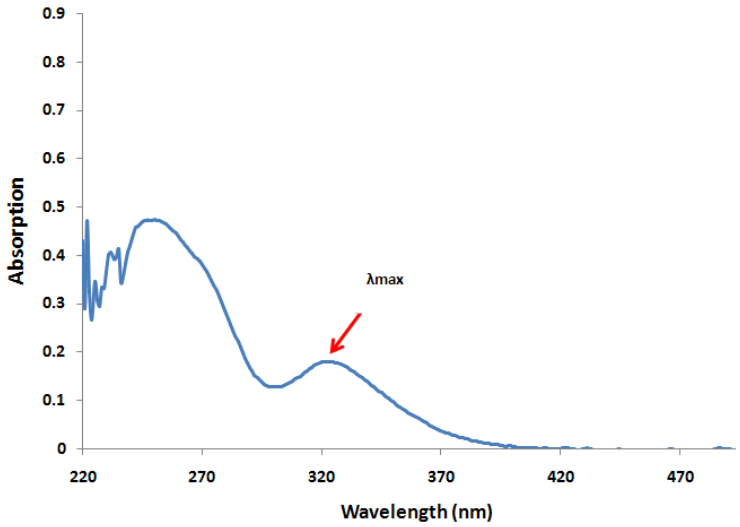

Fig. 2. UV absorbance spectra of methanolic solution of IDM.

In order to analyze the drug, a calibration curve was constructed with several points (Fig. 3), as absorbance vs. analytes concentration in their range of 1.0×10^{-7} to 2.4×10^{-6} M. The wavelength employed to generate calibration curve was 323. Linear regression results and R^2 are also shown in Fig. 3.

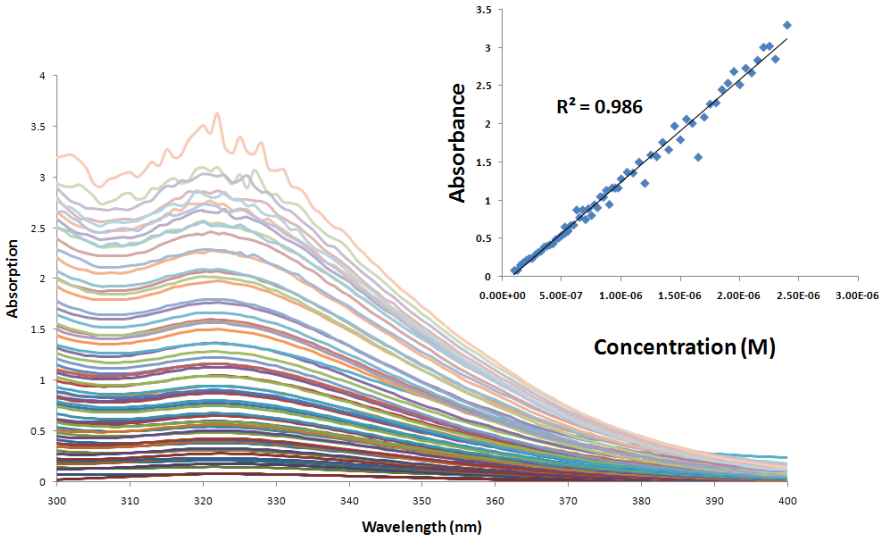

Fig. 3. Absorbance spectra and corresponding calibration curve for univariate determination of IDM.

PCA

Because of the large number of columns of spectra, PCA was employed to solve the collinearity problem in and the principal components (PCs) were used as new variables for model building. After deleting zero variance columns of *X* block, PCA was carried out on the pool of all spectra. A first 10 PCs based on eigenvalue were reported in Table 2. In this Table, the eigenvalues, the percent of variances explained by each eigenvalue and the cumulative percent of variances are represented. After dividing the molecules into two parts, calibration and validation sets, based on Kennard and Stones algorithm, building of regression models using calibration set was performed. 10 first PCs with their eigenvalues are shown in the Table 2. In this Table, the eigenvalues, the percent of variances explained by each eigenvalue and the cumulative percent of variances are represented. PCA gives 2 significant PCs (% variance explained > 1) that can explain 99.98% of the variances in the original descriptors data matrix.

Table 2. Eigenvslues of calculated PCs, % of explained variances and cumulative variances obtained from PCA.

PC No.	Eigenvalue	% variance explained	cumulative variance
1	99.20	98.22	98.22
2	1.78	1.76	99.98
3	0.01	0.01	99.99
4	0.00	0.00	99.99
5	0.00	0.00	100.00

Table 3. The predicted concentrations of IDM and the corresponding relative error of prediction (REP) obtained by PCR and PC-ANN models.

		PCR		PC-ANN	
Training Set	**Concentration**	**Predicted Activity**	**REP**	**Predicted Activity**	**REP**
1	1.00×10^{-7}	1.71×10^{-7}	-7.12×10^{-1}	1.04×10^{-7}	-3.53×10^{-2}
2	1.25×10^{-7}	1.72×10^{-7}	-3.73×10^{-1}	1.17×10^{-7}	6.59×10^{-2}
3	1.50×10^{-7}	2.20×10^{-7}	-4.64×10^{-1}	1.56×10^{-7}	-3.77×10^{-2}
4	1.75×10^{-7}	2.44×10^{-7}	-3.92×10^{-1}	1.87×10^{-7}	-6.71×10^{-2}
5	2.00×10^{-7}	2.67×10^{-7}	-3.35×10^{-1}	2.09×10^{-7}	-4.72×10^{-2}
6	2.25×10^{-7}	2.85×10^{-7}	-2.65×10^{-1}	2.34×10^{-7}	-3.95×10^{-2}
7	2.50×10^{-7}	2.82×10^{-7}	-1.27×10^{-1}	2.27×10^{-7}	9.14×10^{-2}
8	2.75×10^{-7}	3.18×10^{-7}	-1.55×10^{-1}	2.75×10^{-7}	-1.79×10^{-3}
9	3.00×10^{-7}	3.46×10^{-7}	-1.52×10^{-1}	3.02×10^{-7}	-6.74×10^{-3}
10	3.25×10^{-7}	3.58×10^{-7}	-1.02×10^{-1}	3.28×10^{-7}	-8.65×10^{-3}
11	3.50×10^{-7}	3.93×10^{-7}	-1.24×10^{-1}	3.57×10^{-7}	-1.97×10^{-2}
12	3.75×10^{-7}	4.04×10^{-7}	-7.75×10^{-2}	3.74×10^{-7}	1.45×10^{-3}
13	4.00×10^{-7}	4.16×10^{-7}	-4.7×10^{-2}	3.84×10^{-7}	4.05×10^{-2}
14	4.25×10^{-7}	4.28×10^{-7}	-6.94×10^{-3}	4.7×10^{-7}	4.32×10^{-2}
15	4.50×10^{-7}	4.61×10^{-7}	-2.43×10^{-2}	4.37×10^{-7}	2.94×10^{-2}
16	4.75×10^{-7}	4.86×10^{-7}	-2.41×10^{-2}	4.82×10^{-7}	-1.50×10^{-2}
17	5.00×10^{-7}	5.09×10^{-7}	-1.79×10^{-2}	4.90×10^{-7}	1.98×10^{-2}
18	5.25×10^{-7}	5.28×10^{-7}	-5.03×10^{-3}	5.26×10^{-7}	-2.26×10^{-3}
19	5.50×10^{-7}	5.54×10^{-7}	-7.18×10^{-3}	5.47×10^{-7}	6.12×10^{-3}
20	5.25×10^{-7}	5.90×10^{-7}	-1.23×10^{-1}	5.96×10^{-7}	-1.35×10^{-1}
21	5.50×10^{-7}	5.51×10^{-7}	-1.27×10^{-3}	5.43×10^{-7}	1.25×10^{-2}
22	5.75×10^{-7}	6.04×10^{-7}	-4.96×10^{-2}	6.13×10^{-7}	-6.70×10^{-2}
23	6.00×10^{-7}	6.14×10^{-7}	-2.30×10^{-2}	6.18×10^{-7}	-3.08×10^{-2}
24	6.25×10^{-7}	7.43×10^{-7}	-1.89×10^{-1}	7.35×10^{-7}	-1.76×10^{-1}
25	6.50×10^{-7}	6.87×10^{-7}	-5.72×10^{-2}	7.01×10^{-7}	-7.92×10^{-2}
26	6.75×10^{-7}	7.43×10^{-7}	-1.01×10^{-1}	7.35×10^{-7}	-8.88×10^{-2}
27	7.00×10^{-7}	6.66×10^{-7}	4.85×10^{-2}	6.75×10^{-7}	3.56×10^{-2}
28	7.25×10^{-7}	7.58×10^{-7}	-4.49×10^{-2}	7.49×10^{-7}	-3.35×10^{-2}
29	7.50×10^{-7}	7.06×10^{-7}	5.90×10^{-2}	7.20×10^{-7}	3.94×10^{-2}
30	7.75×10^{-7}	7.98×10^{-7}	-3.00×10^{-2}	7.95×10^{-7}	-2.56×10^{-2}
31	8.00×10^{-7}	7.81×10^{-7}	2.37×10^{-2}	7.99×10^{-7}	1.20×10^{-3}
32	8.25×10^{-7}	8.71×10^{-7}	-5.63×10^{-2}	8.67×10^{-7}	-5.08×10^{-2}
33	8.50×10^{-7}	8.85×10^{-7}	-4.14×10^{-2}	9.21×10^{-7}	-8.34×10^{-2}
34	8.75×10^{-7}	9.35×10^{-7}	-6.85×10^{-2}	9.40×10^{-7}	-7.40×10^{-2}
35	9.00×10^{-7}	8.13×10^{-7}	9.71×10^{-2}	8.37×10^{-7}	7.04×10^{-2}
36	9.25×10^{-7}	9.54×10^{-7}	-3.19×10^{-2}	9.53×10^{-7}	-3.00×10^{-2}
37	9.50×10^{-7}	9.71×10^{-7}	-2.21×10^{-2}	9.96×10^{-7}	-4.85×10^{-2}
38	9.75×10^{-7}	9.58×10^{-7}	1.76×10^{-2}	9.65×10^{-7}	1.08×10^{-2}
39	1.00×10^{-6}	1.05×10^{-6}	-4.68×10^{-2}	1.04×10^{-6}	-4.47×10^{-2}

Table 3 (Continued)

		PCR		PC-ANN	
Training Set	**Concentration**	**Predicted Activity**	**REP**	**Predicted Activity**	**REP**
40	1.05×10^{-6}	1.11×10^{-6}	-5.42×10^{-2}	1.11×10^{-6}	-6.16×10^{-2}
41	1.10×10^{-6}	1.7×10^{-6}	3.10×10^{-2}	1.09×10^{-6}	7.00×10^{-3}
42	1.15×10^{-6}	1.19×10^{-6}	-3.67×10^{-2}	1.19×10^{-6}	-3.76×10^{-2}
43	1.20×10^{-6}	1.02×10^{-6}	1.48×10^{-1}	1.08×10^{-6}	1.00×10^{-1}
44	1.25×10^{-6}	1.27×10^{-6}	-1.39×10^{-2}	1.27×10^{-6}	-1.92×10^{-2}
45	1.30×10^{-6}	1.28×10^{-6}	1.44×10^{-2}	1.35×10^{-6}	-4.12×10^{-2}
46	1.35×10^{-6}	1.39×10^{-6}	-2.82×10^{-2}	1.40×10^{-6}	-3.62×10^{-2}
47	1.40×10^{-6}	1.34×10^{-6}	4.38×10^{-2}	1.37×10^{-6}	2.03×10^{-2}
48	1.45×10^{-6}	1.54×10^{-6}	-5.95×10^{-2}	1.55×10^{-6}	-6.85×10^{-2}
49	1.50×10^{-6}	1.44×10^{-6}	3.67×10^{-2}	1.53×10^{-6}	-1.86×10^{-2}
50	1.55×10^{-6}	1.62×10^{-6}	-4.27×10^{-2}	1.63×10^{-6}	-5.32×10^{-2}
51	1.60×10^{-6}	1.61×10^{-6}	-4.11×10^{-3}	1.68×10^{-6}	-5.24×10^{-2}
52	1.65×10^{-6}	1.25×10^{-6}	2.42×10^{-1}	1.27×10^{-6}	2.33×10^{-1}
53	1.70×10^{-6}	1.63×10^{-6}	4.13×10^{-2}	1.64×10^{-6}	$3.24\times10_{-2}$
54	1.75×10^{-6}	1.77×10^{-6}	-1.03×10^{-2}	1.79×10^{-6}	-2.18×10^{-2}
55	1.80×10^{-6}	1.78×10^{-6}	1.22×10^{-2}	1.78×10^{-6}	9.06×10^{-3}
56	1.85×10^{-6}	1.90×10^{-6}	-2.45×10^{-2}	1.90×10^{-6}	-2.67×10^{-2}
57	1.90×10^{-6}	1.96×10^{-6}	-3.12×10^{-2}	1.95×10^{-6}	-2.44×10^{-2}
58	1.95×10^{-6}	2.04×10^{-6}	-4.38×10^{-2}	2.02×10^{-6}	-3.70×10^{-2}
59	2.00×10^{-6}	1.96×10^{-6}	2.17×10^{-2}	1.94×10^{-6}	2.82×10^{-2}
60	2.05×10^{-6}	2.09×10^{-6}	-2.02×10^{-2}	2.7×10^{-6}	-1.10×10^{-2}
61	2.10×10^{-6}	2.10×10^{-6}	3.23×10^{-4}	2.13×10^{-6}	-1.47×10^{-2}
62	2.15×10^{-6}	2.17×10^{-6}	-1.08×10^{-2}	2.13×10^{-6}	7.30×10^{-3}
63	2.20×10^{-6}	2.34×10^{-6}	-6.36×10^{-2}	2.26×10^{-6}	-2.57×10^{-2}
64	2.25×10^{-6}	2.26×10^{-6}	-6.12×10^{-3}	2.20×10^{-6}	2.23×10^{-2}
65	2.30×10^{-6}	2.17×10^{-6}	5.68×10^{-2}	2.20×10^{-6}	4.41×10^{-2}
66	2.40×10^{-6}	2.52×10^{-6}	-4.90×10^{-2}	2.42×10^{-6}	-9.05×10^{-3}

PCR modeling

After acquiring PCs, linear regression was performed. The obtained model consists of 3 terms, with one constant term and 2 terms based on different PCs. The model is given by the following equation:

Concentration = $(10.35\times10^{-6}) + (64.54\times10^{-8}\times PC_1) - (53.21\times10^{-8}\times PC_2)$

N =46; R^2 = 0.982

Where N is the number of solutions in the calibration set. The experimental and predicted values of concentration for each solution and the corresponding relative errors of the predicted concentration (*REP*) are reported in Table 3.

The correlation between experimental and predicted values of concentration of both the calibration and test sets obtained by the PCR modeling is presented graphically in Fig. 4A. This figure shows clearly that the obtained PCR model works well over the entire range of the concentration values.

Furthermore, corresponding values of the test set solutions fall close to the values and the trend line of the calibration set, well within the error bars evaluated and reported in above equation. A correlation coefficient of this plot indicates the reliability of the model. The residuals of the PCR calculated values of concentrations are plotted against the experimental values in Fig. 3B. The propagation of the residuals on both sides of zero line indicates that no symmetric error exists in the development of the PCR model.

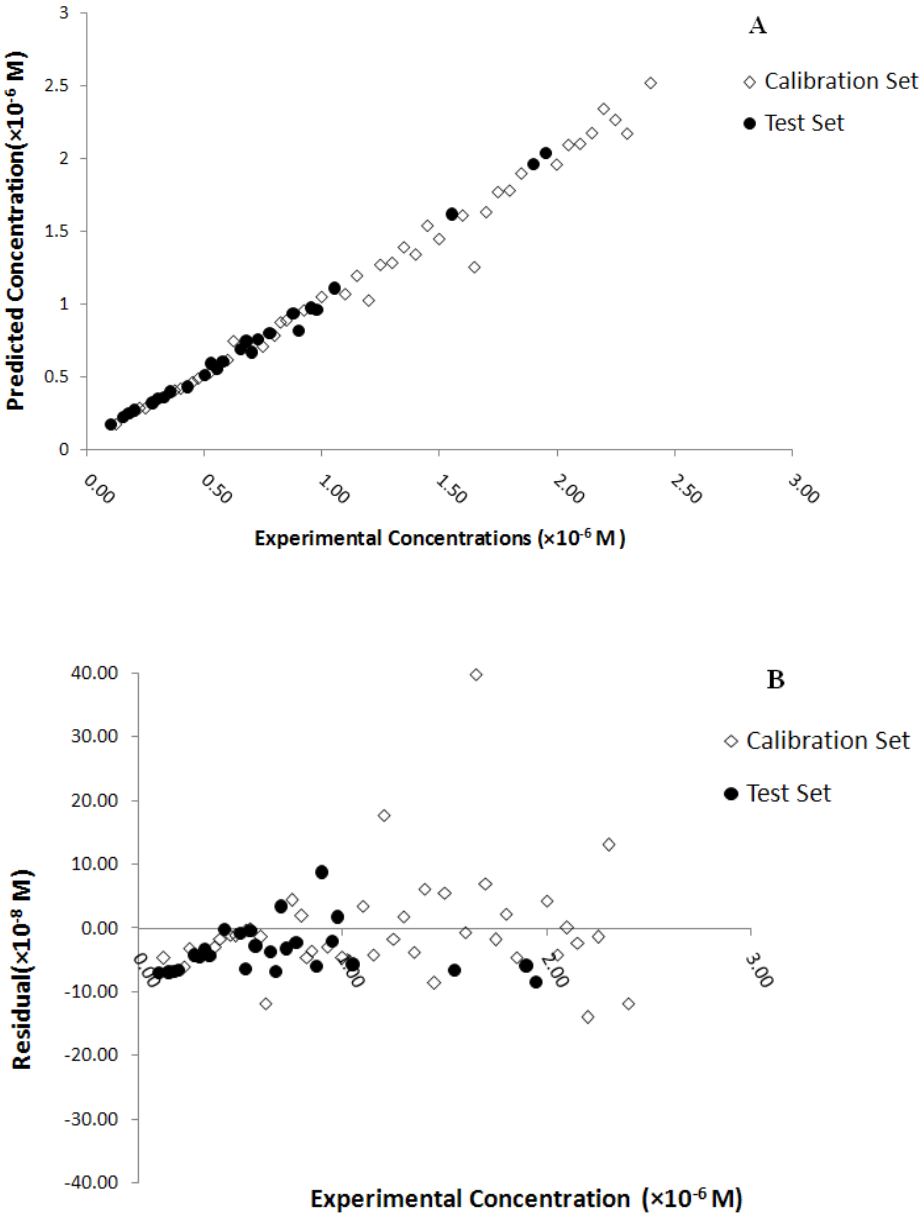

Fig. 4. (A) Predicted concentration vs. experimental concentration and, (B) Residual vs. experimental concentration for PCR model.

Leave-one-out cross-validation (LOO) is an accepted method applied to find the reliability of the generated models. In this validation, a number of modified datasets (equal to the number of the studied solutions) are prepared by removing one of the solutions at a time [21-23], and generating a model for each dataset by means of the same modeling procedure adopted in the modeling step. Each model is examined through the evaluation of its power in predicting the concentration of the left-out solution. This process is repeated until a complete set of predicted concentration for all investigated solutions in calibration set is achieved.

To evaluate the predictive ability and to check the statistical significance of the developed PCR model, the proposed model was used for prediction of concentration values of for external set that were not used in model building. The root mean square error cross-validation (*RMSEcv*) is calculated as a standard index to estimate the accuracy of the modeling which is based on the cross-validation technique and the set of R^2_{LOO} (correlation coefficient of leave-one-out). According to Tropsha et al., [17], the high value of R^2_{LOO} is necessary, but not sufficient condition for the developed model to have a high predictability. In addition to a high R^2_{LOO} , a reliable model should also be characterized by a high correlation coefficient of regression R^2between the calculated and experimental values of compounds from a test set [24]. If the R^2_{LOO}> 0.5 and R^2> 0.6 criteria suggested by Tropsha et al. [17] are satisfied, then it can be said that the model is predictive.

Therefore, the developed model is validated by some statistics parameters explained above and results are reported in the Table 4.

As it is shown in the Table 4, R^2 that is a criterion of goodness of fit of proposed model was obtained for two sets. The high value of this parameter indicates a good fit between experimental activity and predicted values of antagonist activities of compounds by developed model. This shows the high capability of the proposed model. As it can be seen from this table, the PCs used in this model can explain 98.20% of the variances in the concentrations of the solutions used in this study. The external predictability and model capability of a proposed model is generally tested using test set and leave one out cross validation. The satisfactory prediction of values of inhibitory activity of test set solutions demonstrates the efficacy of the PCR model in predicting activities of external set solutions. Moreover, the low values of *RMSE* for prediction of IMD concentration of plasma samples in test set increases the statistical significance of the developed model.

PC-ANN modeling

To increase the predictability of the developed models obtained between the PCs and solution concentrations, a non-linear modeling method was also developed in this study. Usually, superior models can be constructed using ANNs because they implement non-linear relationships and also they have more adjustable parameters than the typical linear models. As discussed, a fully connected, three-layered feed-forward ANN model with back-propagation [25] learning algorithm was used. In the same manner as PCR analysis, eigenvalue ranking was used to sort the most relevant set of PCs as input of ANN. The most important set of PCs used in PCR analysis (i.e. PC1 and PC2) was selected based on their eigenvalues. This subset of PCs can be employed as input of ANN model.

Overfitting problem or poor generalization capability takes place when an ANN over learns during the training stage of network. An overfitted ANN model may not carry out well on unseen data set due to its lack of generalization capability. On other words, if over-training does happen, contributions of a small subset of the training set solutions may be considered as a major contribution, thus hindering the ability of the developed PC-ANN model to accurately predict the concentration of solution of interest. An efficient way to overcome this problem is the early stopping technique in which the training process is terminated as soon as the overtraining signal appears. This method needs the data set to be divided into three subsets: training set, test set, and validation sets. The training and the validation sets are the norm in all model training processes. The test set is used to test the trend of the prediction accuracy of the developed ANN model trained at some point of the training stage.

At later training stages, the validation error increases. This is the point when the model should cease to be trained to overcome the overfitting problem. To achieve this purpose, the extracted PCs were divided three sets: training set (65%), validation set (15%), and external prediction (or test) set (20%). Then, the training and validation sets were employed to optimize the network performance. The regression between the PC-ANN output and the concentration was estimated for the three sets individually. To build PC-ANN models with lower RMSE, the neural code written was run many times, each time run with different number of neurons in hidden layer and/or initial weights.

Table 4. Statistical parameters and figures of merit for different sets using developed PCR and PC-ANN models.

	PCR			**PC-ANN**			
Statistics	**Training Set**	**Test Set**	**Total**	**Training Set**	**Validation Set**	**Test Set**	**Total**
N	40	26	66	43	10	13	66
R^2	0.982	0.994	0.987	0.987	0.998	0.993	0.990
RMSE (M)	8.71×10^{-08}	5.20×10^{-08}		7.42×10^{-08}	3.30×10^{-08}	5.05×10^{-08}	6.57×10^{-08}
R^2_{CV}	0.980			0.993			
$RMSE_{CV}$ *(M)*	9.36×10^{-08}			8.66×10^{-08}			
%ERR	5.95	12.69		6.25	10.97	5.49	
Linear Range (M)	1×10^{-7} to 2.4×10^{-6}			1×10^{-7} to 2.4×10^{-6}			
LOD (M)	0.25×10^{-7}			0.21×10^{-7}			
LOQ (M)	0.83×10^{-7}						

Practical applications of a typical ANN model need some way of selecting the number of nodes in hidden layer, and other specifications such as the learning rate and momentum term. The correct optimization of these parameters separates the signal from the noise and avoid over-fitting of the model. A typical ANN model can consequently be characterized by their architecture,

The two PCs were examined with several ANN architectures. The developed PC-ANN models were considered with a single hidden layer. In hidden layer a sigmoid transfer function, as a more versatile transfer function, was applied. Each connection in the developed PC-ANN is made up of a weighting factor and a bias term. The weights and biases are optimized during training based on the MSE of the test set (*MSEtest*); the corresponding value is then estimated for the validation set for each of geometry. In each ANN, the neuron architecture (i.e. the number of nodes in hidden layer; n_H) ,parameters (i.e. learning rate and momentum) and number of learning iterations (epochs) were optimized to reach the lowest MSE as the performances of the resulted PC-ANN models, because it is believed that overtraining occurs when the MSE begins to rise. At this point, the values of the weights and biases are not further changed.

In order to establish the optimum number of neurons in hidden layer several training runs were conducted with different number of hidden neurons.

A response surface methodology was applied to optimize number of neurons in hidden layer and number of epochs. The value of MSE for test set was calculated and recorded after every 100 cycles and for a total of 1000 epochs. The calculated values of MSE for test set were plotted

against the number of nodes in hidden layer and number of epoch, from which the optimum values of these parameters with minimum value of MSE was determined (Fig. 5). It can be seen from this figure that 3 neurons in hidden layer and 600 epochs were sufficient for a good performance of the PC-ANN.

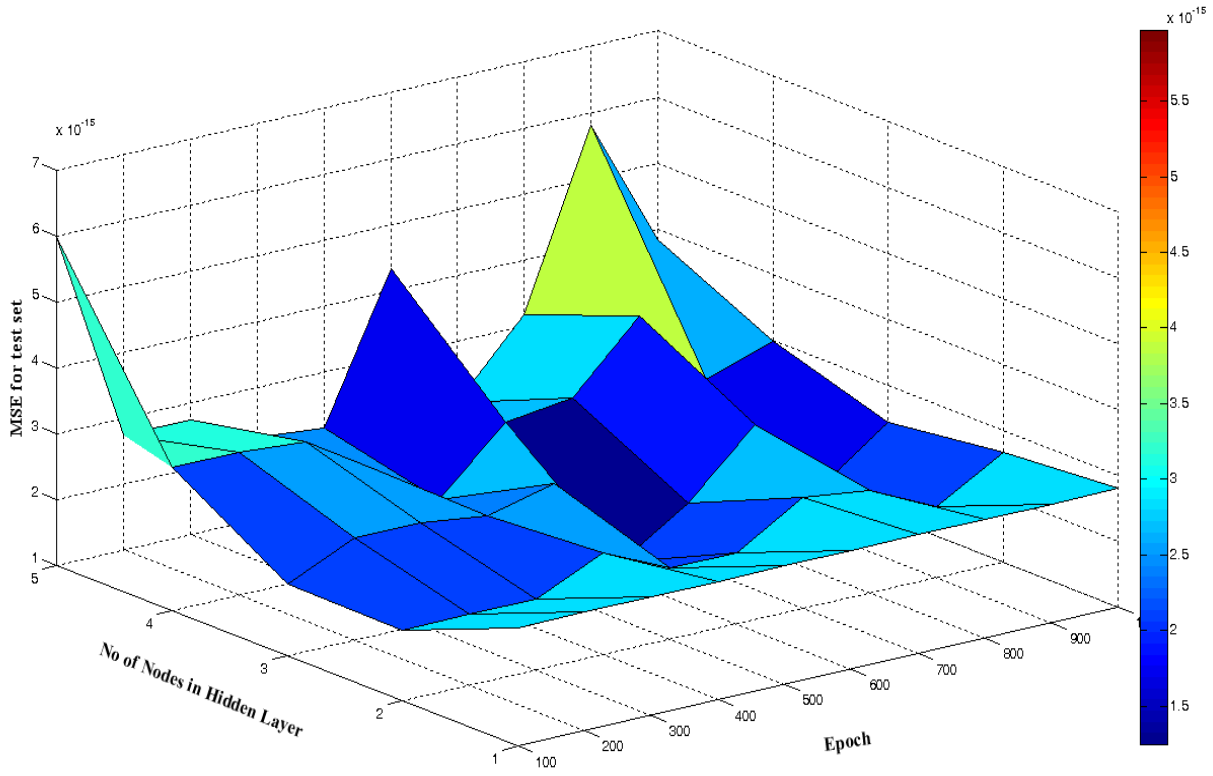

Fig. 5. Optimization of number of epoch and number of neurons in hidden layer for developed PC-ANN model.

One of the most important factors for backpropagation learning is the learning rate of the developed ANN as it determines the size of the weight changes. Smaller learning rates slow the learning process, while larger rates cause the error function to change wildly without continuously improving. Said another way, the learning rate in a parameter that determines the size of the weights adjustment each time the weights are changed during training. Small values for the learning rate cause small weight changes and large values cause large changes.

The best learning rate is not obvious. If the learning rate is 0.0, the ANN will not learn.

To improve the learning procedure a momentum parameter is employed which permits for larger learning rates. The parameter determines how past weight changes affect current weight changes, by making the next weight change in approximately the same direction as the previous one.

A response surface methodology was also applied to optimize learning rate and momentum parameters [26] .The surface plot of MSE as a function of linear rate and momentum in three different numbers of nodes in hidden layer is shown in Fig. 6. The results show that an ANN with 2 PCs as input variables, 3 nodes in its hidden layer (2-3-1 architecture), learning rate of 0.7, and momentum of 0.1 resulted in the optimum PC-ANN performance. The network was trained using calibration samples and it was assessed by prediction set.

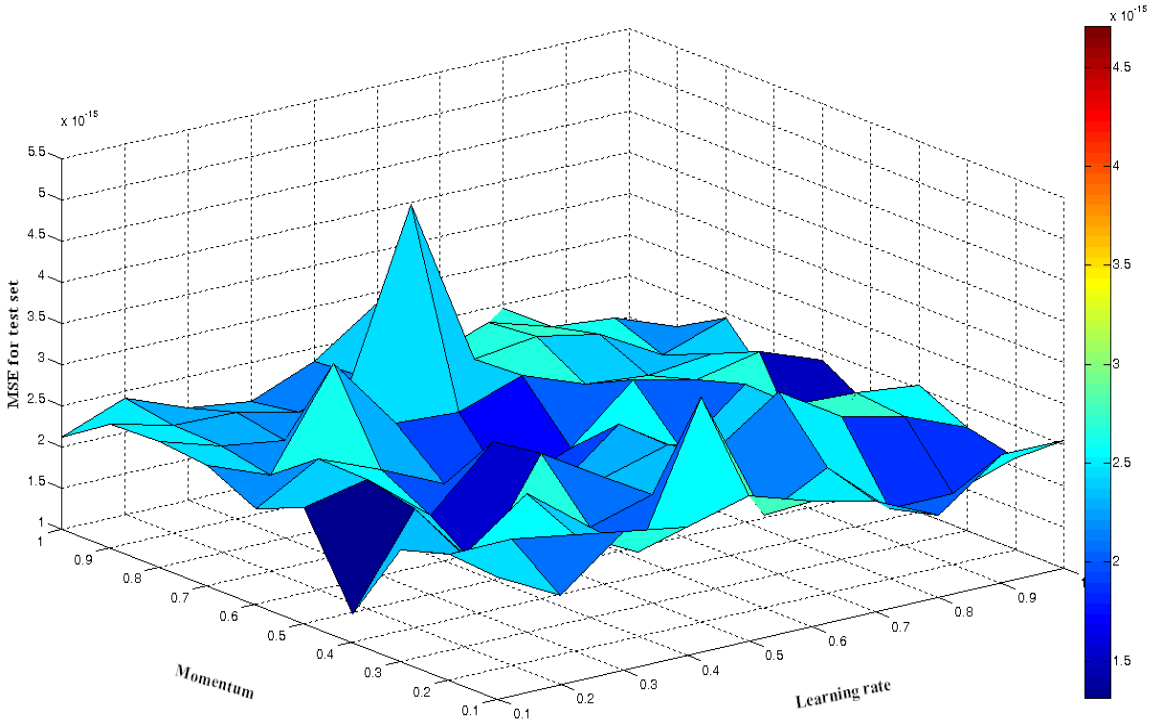

Fig. 6. Optimization of linear rate and momentum for developed PC-ANN model

The results of the ANN-based non-linear correlation between two first extracted PCs and concentration of solutions and REP is represented in Table 3.

Fig. 7A indicates the plot of the PC-ANN calculated versus the experimental values of the concentrations for the studied data set. A correlation coefficient of this plot shows the trustworthiness of the generated model. The residuals of the PC-ANN calculated values of concentration are plotted for each of solutions in Fig. 7B. The spread of the residual values on both sides of zero line shows that no symmetric error exists in the development of the PC-ANN model. As can be seen in this figure, the residuals of PC-ANN are smaller than that of PCR.

The predictive ability of the developed PC-ANN model was verified by Leave-One-Out cross validation technique, where one object (molecule) is deleted at once and prediction of the activity of the deleted solution is made based on the developed PC-ANN model. The square of correlation coefficient and *RMSEcv* values of the model are shown in Table 4.

The robust and highly predictive ability of the generated model was expressed inadequately only by the cross validation method, thus the external predictive power of the model was evaluated with the prediction set solutions. The predictive power of the model is calculated also by R^2_{Pred}. The high R^2_{Pred} value of 0.994 (R^2 for test set in Table 4) account for good predictability. The developed PC-ANN model thus was robust and was establish satisfactory for predicting the IDM concentration of the test set.

According to PC-ANN, it can explain and predict 98.2% and 99.4% of absorbance spectra, respectively, which can be proved in predicting the test set.

This means that in agreement with our previous studies the developed PC-ANN is moderately more accurate compared with that of the simple linear regression using PCs [20, 27-29].

For a given model, internal validation, although essential and obligatory, does not adequately assure the predictability of a model. In fact, we are strongly persuaded from previous experience that

models with high apparent predictability, emphasized only by internal validation approaches, can be unpredictive when confirmed on new compounds not applied in developing the model. Thus, for a stronger assessment of model applicability for prediction on new samples, external validation of the generated model should always be carried out.

In the present study, the quality of the model was assessed by prediction of concentration of IDM in samples of test set. Results are shown in Table 3 and figure 7A and 7B.

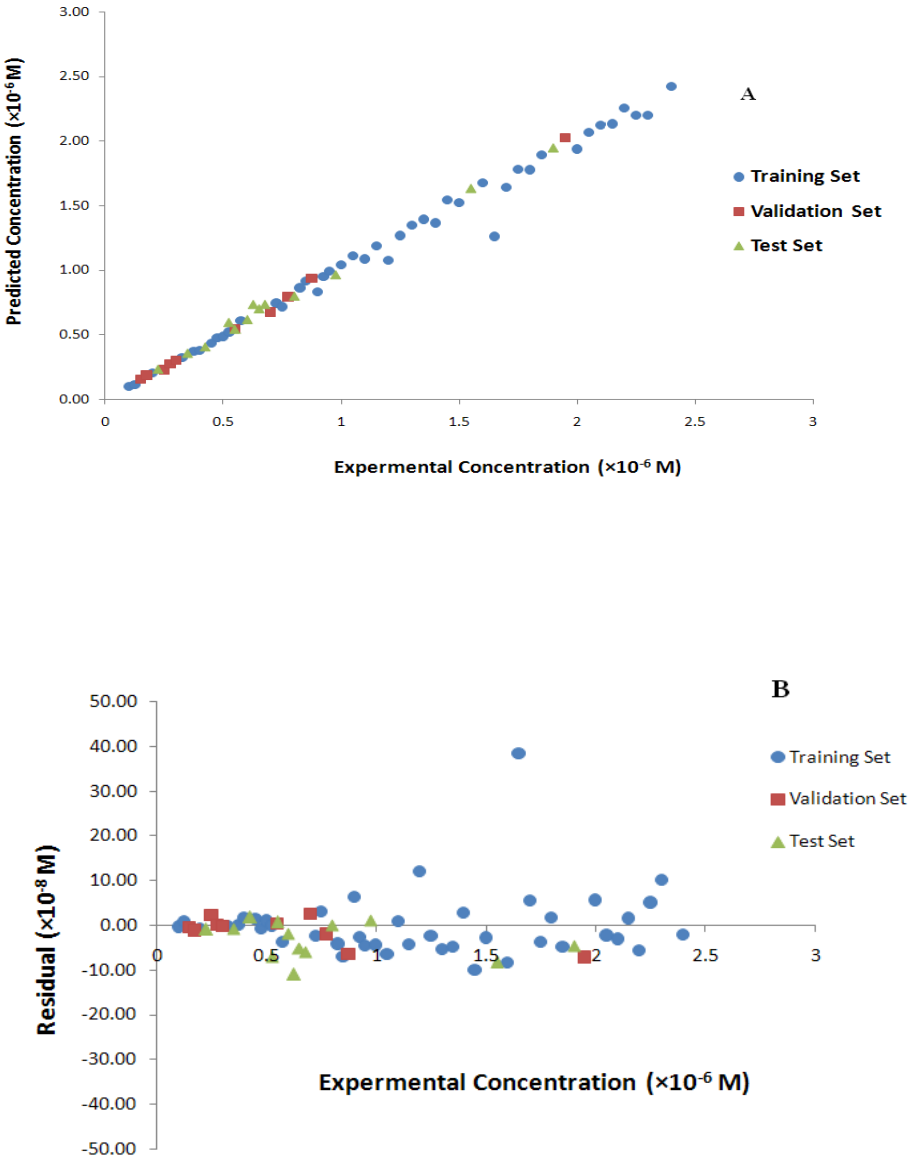

Fig. 7. (A) Predicted concentration *vs.* experimental concentration and, (B) Residual *vs.* experimental concentration for PC-ANN model.

The good correlation coefficient (0.987 for training set, 0.998 for validation set, and 0.993 for test set) reveals the capability of the model.

The statistical quantities of the calibration model obtained by PC-ANN model, applying on whole spectral range, are reported in Table 4.

The linear dynamic range was the same PCR. In this report, the detection limit has been estimated from the univariate definition as described by Garcia et al [30] and Ketterer et al. [31]. The absorbance spectra for five blank solutions was obtained under condition described. From the PC-ANN modeling, the predicted concentrations for IDM were calculated. The standard deviation of predicted concentrations for IDM was calculated (S_b). Then, three times the S_b for IDM was taken as the detection limit. Detection limit was 0.21×10^{-7} M.

The number of PCs used to model absorbance spectra–concentration is higher than the number of analytes, which can be attributed to the interaction between the serum components.

The goodness of the fit for the resulted PC-ANN model can be measured by cross-validation statistics such as *RMSE* for cross-validation (*RMSEcv*), and cross-validated square of correlation coefficient (R^2_{CV}). The root mean square error for training is also included in Table 4 for comparison between two models.

Precision and accuracy

The procedures described above were repeated five times within the day to determine the repeatability (intra-day precision) and five times on different days of week to determine the intermediate precision (inter-day precision) of the developed model. The percentage relative standard deviation (%RSD) values were ≤ 1.87 % (intra-day) and ≤ 1.92 % (inter-day) indicating high precision of the methods. Accuracy was evaluated as percentage relative error (*RE*) between the measured mean concentrations and taken concentrations for IDM. Percent relative error or Bias (bias % = [(Concentration found - known concentration) × 100 / known concentration]) was calculated at each concentration. The Percent relative error values were ≤ 3 % (intra-day) and ≤ 1.94 % (inter-day) indicating high precision of the methods. Percent relative error (%RE) values of ≤ 2.5 % demonstrate the high accuracy of the proposed methods.

Comparison of the results of PC-ANN with HPLC

In order to assess the results of the PC-ANN model as superior chemometrics model, a HPLC procedure was also used to analyze the IDM in the plasma samples. At the optimized conditions, the retention time for IDM was 5.26 min.

One component analysis showed that the chromatographic responses were linear in the concentration ranges, which is lower than what is used in the PC-ANN procedure.

Two sets of standard solutions resulted from synthetic mixtures of drugs spiked in the plasma were also used in HPLC experiment.

The calibration set was employed to construct the calibration curve, and the resulted calibration equation was employed to predict the concentration of the IDM in the prediction set.

The approach was validated with regards to linearity, limit of detection and quantification, recovery, precision, accuracy and specificity.

Peak area (Y) of IDM of calibration standards was proportional to the concentration (x) of drugs in plasma over the range tested. The peak area ratio (Y) of IDM calibration standards was proportional to the concentration (x) of IDM in plasma over the range tested. Blank human blood samples spiked with the corresponding compounds to give concentrations of 1.40, 2.79, 4.19, 5.59 and 6.98 $\times 10^{-8}$ M were analyzed. For all analytes, excellent linearity was obtained in the specified concentration range.

As it can be seen in figure 8, the correlation coefficient for the calibration regression line was 0.990.

The LOQ and the LOD of IDM was estimated to be 0.69×10^{-7}M and 0.21×10^{-7} M.

The reproducibility of the HPLC was nearly the same as that of used chemometrics methods. However, the calculated theoretical IDM of HPLC (0.42 M) was lower than those of PCR and PC-ANN.

The data supports that the prediction ability of the HPLC method and PC-ANN method is not very significant. Similar to those found by PC-ANN, HPLC has generated very accurate results and the recoveries for IDM in plasma samples. Statistical Student's t-test indicates that at a significance

level of 95% there are not significant differences between the predicted values by two methods.The data supports that the analytical power and prediction ability of the HPLC method is relatively higher than that of the ANN model, but, the differences are not very significant.

Conclusion

Determination of indomethacin performed directly by spectrophotometric measurements using chemometric modeling.
Two models (PCR) and (PCANN) were developed and optimized. The PC-ANN method was used to the determination of indomethacin successfully. This study showed that the combination of PCA and ANN is efficient method for determination of Indomethacin in plasma.
High analytical potential of the ANNs created satisfactory results. The structure of the PC-ANN was simplified by using the corresponding important PCs as input variables instead of original spectral data. Totally, comparison of constructed models than those obtained by ANN, dramatically, lower *RMSEP*% values. The methods offer good procedures for the analyzing of complex mixtures such plasma, using simple spectrophotometer, which is available in most laboratories and without any separation steps.
Generalisation ability of the PC-ANN model is confirmed by its ability in predicting the concentration of IDM, i.e. a solution not included in the set of test solution used in training of PC-ANN model. Again, although PCR provide moderate *R* value, ANN gives a lower ERR% in prediction (4.4% versus 12.8%). This procedure guarantees high recoveries and good extraction repeatability.

Acknowledgments

The authors are grateful to the Vice Chancellor for Research and Technology, Kermanshah University of Medical Sciences for the financial support (Research Grant No. 92283). This article resulted from the Pharm. D thesis of Hamid Nabiyar, Major of Pharmacy, Kermanshah University of Medical Sciences, Kermanshah, Iran.

Conflict of interest

Authors certify that no actual or potential conflict of interest in relation to this article exists.

References

[1] Michail K, Moneeb MS. Determination of methotrexate and indomethacin in urine using SPE-LC-DAD after derivatization. J.pharm. biomed. anal. 2011;55:317-324.
[2] Bakkali A, Corta E, Berrueta L, Gallo B, Vicente F. Study of the solid-phase extraction of diclofenac sodium, indomethacin and phenylbutazone for their analysis in human urine by liquid chromatography. J. Chromatogr. B. 1999;729:139-145.
[3] Moore C, Tebbett I. Rapid extraction of anti-inflammatory drugs in whole blood for HPLC analysis. Forensic sci. int. 1987;34:155-158.
[4] Smith PC, Benet LZ. High-performance liquid chromatographic method for the determination of indomethacin and its two primary metabolites in urine. J. Chromatogr. B. 1984;306:315-321.
[5] Al Za'abi M, Dehghanzadeh G, Norris R, Charles B. A rapid and sensitive microscale HPLC method for the determination of indomethacin in plasma of premature neonates with patent ductus arteriousus. J. Chromatogr. B. 2006;830:364-367.
[6] Sato J, Amizuka T, Niida Y, Umetsu M, Ito K. Simple, rapid and sensitive method for the determination of indomethacin in plasma by high-performance liquid chromatography with ultraviolet detection. J. Chromatogr. B. 1997;692:241-244.
[7] Niopas I, Mamzoridi K. Determination of indomethacin and mefenamic acid in plasma by high-performance liquid chromatography. J. Chromatogr. B. 1994;656:447-450.
[8] Cooper J, McKay G, Hawes E, Midha K. High-performance liquid chromatographic assay of indomethacin and its application in pharmacokinetics in healthy volunteers J. Chromatogr. B. 1982;233:289-296.
[9] Bayne W, East T, Dye D. High-pressure liquid chromatographic method with postcolumn, in-line hydrolysis and fluorometric detection for indomethacin in biological fluids. J. pharm. sci. 1981;70:458-459.
[10] Taylor PJ, Jones CE, Dodds HM, Hogan NS, Johnson AG. Plasma indomethacin assay using high-performance liquid chromatography-electrospray-tandem mass spectrometry: application to therapeutic drug monitoring and pharmacokinetic studies. Ther. drug monit. 1998;20:691-696.

[11] Rezaei Z, Hemmateenejad B, Khabnadideh S, Gorgin M. Simultaneous spectrophotometric determination of carbamazepine and phenytoin in serum by PLS regression and comparison with HPLC. Talanta. 2005;65:21-28.
[12] Shahlaei M, Andisheh H, Derakhshandeh K, Sadrjavadi K. A novel method for simultaneous determination of codeine and acetaminophen in plasma by combination of UV-Vis spectroscopy and artificial neural network. J. Rep. Pharm. Sci. 2014;3:141-158.
[13] Shahlaei M, Hassanzadeh F, Sohrabi E, Emami J, Saghaie L. Simultaneous Spectrophotometric Determination of Amlodipine and Metoprolol by Principal Componentregression Multivariate Calibration and Comparison With HPLC. J. Rep. Pharm. Sci. 2013;2:179-189.
[14] Paleologos EK, Prodromidis MI, Giokas DL, Pappas AC, Karayannis MI. Highly selective spectrophotometric determination of trace cobalt and development of a reagentless fiber-optic sensor. Anal. Chim. Acta. 2002;467:205-215.
[15] Abdollahi H. Simultaneous spectrophotometric determination of chromium (VI) and iron (III) with chromogenic mixed reagents by H-point standard addition method and partial least squares regression. Anal. Chim. Acta. 2001;442:327-336.
[16] Afkhami A, Abbasi-Tarighat M, Khanmohammadi H. Simultaneous determination of Co2+, Ni2+, Cu2+ and Zn2+ ions in foodstuffs and vegetables with a new Schiff base using artificial neural networks. Talanta. 2009;77:995-1001.
[17] Tropsha A, Gramatica P, Gombar VK. The importance of being earnest: validation is the absolute essential for successful application and interpretation of QSPR models. QSAR Comb. Sci. 2003;22:69-77.
[18] Kennard R, Stone L. Computer Aided Design of Experiments. Technometrics. 1969;11:137-148.
[19] Ni Y, Chen S, Kokot S. Spectrophotometric determination of metal ions in electroplating solutions in the presence of EDTA with the aid of multivariate calibration and artificial neural networks. Anal. Chim. Acta. 2002;463:305-316.
[20] Shahlaei M, Fassihi A, Saghaie L. Application of PC-ANN and PC-LS-SVM in QSAR of CCR1 antagonist compounds: a comparative study. Eur. J. Med. Chem. 2010;45:1572-1582.
[21] Shen M, Béguin C, Golbraikh A, Stables JP, Kohn H, Tropsha A. Application of predictive QSAR models to database mining: identification and experimental validation of novel anticonvulsant compounds. J. Med. Chem. 2004;47:2356-2364.
[22] Shahlaei M, Nazari Z. Computational neural network analysis of the affinity of 2-pyridyl-3, 5-diaryl pyrroles analogs for the human glucagon receptor using density functional theory. Med. Chem. Res. 2014;23:2046-2061.
[23] Shahlaei M, Nazari Z. Prediction of glucagon receptor antagonist activities of some substituted imidazoles using combined radial basis function neural network and density functional theory. Med. Chem. Res. 2014;23:2744-2756.
[24] Golbraikh A, Tropsha A. Beware of q^2! J. Mol.Graph. Model. 2002;20:269-276.
[25] Rummelhart D. Learning representations by back-propagating errors. Nature. 1986;323:533-536.
[26] Shamsipur M, Ghavami R, Sharghi H, Hemmateenejad B. Highly correlating distance/connectivity-based topological indices: 5. Accurate prediction of liquid density of organic molecules using PCR and PC-ANN. J. Mol.Graph. Model. 2008;27:506-511.
[27] Shahlaei M, Sabet R, Ziari MB, Moeinifard B, Fassihi A, Karbakhsh R. QSAR study of anthranilic acid sulfonamides as inhibitors of methionine aminopeptidase-2 using LS-SVM and GRNN based on principal components. Eur. J. Med. Chem. 2010;45:4499-4508.
[28] Shahlaei M, Madadkar-Sobhani A, Fassihi A, Saghaie L, Arkan E. QSAR study of some CCR5 antagonists as anti-HIV agents using radial basis function neural network and general regression neural network on the basis of principal components. Med. Chem. Res. 2012;21:3246-3262.
[29] Shahlaei M, Nowroozi A, Khodarahmi R. A Combined DFT and QSAR Calculations to Study Substituted Biphenyl imidazoles as Bombesin Receptor Subtype-3 Agonists. Lett. Drug Des. Discov. 2014;11:665-676.
[30] Toribio M, Garcia J, Izquierdo-Ridorsa A, Tauler R, Rauret G. Simultaneous determination of plutonium alpha emitters by liquid scintillation counting using multivariate calibration. Anal. Chim. acta. 1995;310:297-305.
[31] Ketterer ME, Reschl JJ, Peters MJ. Multivariate calibration in inductively coupled plasma mass spectrometry. Anal. Chem. 1989;61:2031-2040.

